

Camera Adversarial Transfer for Unsupervised Person Re-Identification

Guillaume Delorme^{*1}, Xavier Alameda-Pineda¹, Stephane Lathuilière², and Radu Horaud¹

¹Inria Grenoble Rhône-Alpes, France

²University of Trento, Italy

Abstract

Unsupervised person re-identification (Re-ID) methods consist of training with a carefully labeled source dataset, followed by generalization to an unlabeled target dataset, i.e. person-identity information is unavailable. Inspired by domain adaptation techniques, these methods avoid a costly, tedious and often unaffordable labeling process. This paper investigates the use of camera-index information, namely which camera captured which image, for unsupervised person Re-ID. More precisely, inspired by domain adaptation adversarial approaches, we develop an adversarial framework in which the output of the feature extractor should be useful for person Re-ID and in the same time should fool a camera discriminator. We refer to the proposed method as camera adversarial transfer (CAT). We evaluate adversarial variants and, alongside, the camera robustness achieved for each variant. We report cross-dataset ReID performance and we compare the variants of our method with several state-of-the-art methods, thus showing the interest of exploiting camera-index information within an adversarial framework for the unsupervised person Re-ID.

1. Introduction

Person re-identification (Re-ID) is a well-studied retrieval task that consists of associating images of the same person across cameras, places and time. Given a query image of a person, we aim to recover his/her identity (ID) from a set of identity-labeled gallery images. The person Re-ID task is particularly challenging for two reasons. First, the query images correspond to IDs never seen before (i.e. during training). Second, the gallery and the query images are captured under a variety of background scenes, illumination conditions, and viewpoints.

Most Re-ID models assume the availability of heavily

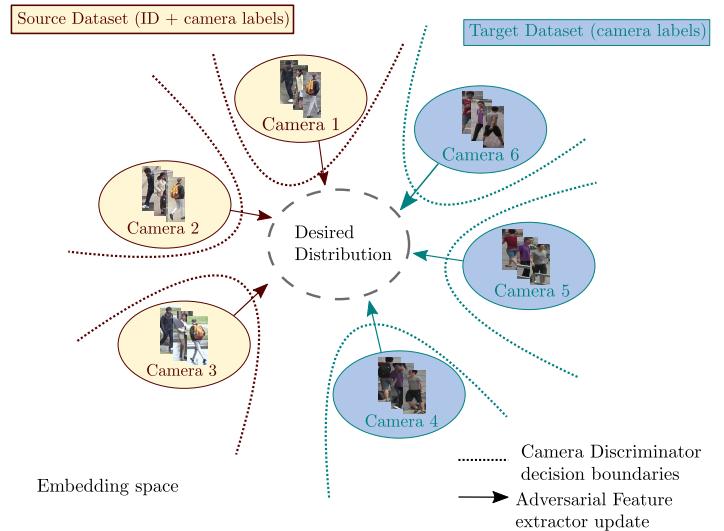


Figure 1. We propose an adversarial method to learn a feature extractor defining an embedding space where the different camera distribution match, and are not distinguishable. To achieve that, we extend the classic adversarial domain adaptation method to a multiple domain formulation, by using a camera-classifier as discriminator, instead of the usual binary classifier. At the same time, we ensure that our features are ID-discriminative by using a standard classification loss.

labeled datasets, and focus on improving their performance on the very same datasets [40, 38, 36, 35, 34, 14]. However, datasets are recorded in specific places and time, and consequently, can be severely biased in terms of background and illumination conditions. These biases partially explain why many Re-ID methods available in the literature generalize poorly to other datasets [6, 5]. Clearly, this reduces their deployability and usability in real-world scenarios. In order to overcome these limitations, several methods were recently proposed attempting to address *unsupervised* person Re-ID [28, 32, 6, 5, 23, 12]. These methods assume the availability of a *source* dataset annotated with person IDs and another unlabeled *target* dataset, and aim to optimize

^{*}Corresponding author: guillaume.delorme@inria.fr

the *target* re-ID performance. In that sense, unsupervised Re-ID is formulated as a domain adaptation problem rather than an unsupervised learning problem.

In parallel, and since generative adversarial networks (GANs) [10] were proposed, adversarial learning has gained popularity in the domain adaptation field [27, 8, 2]. The underlying intuition is that learning a feature generator robust to the domain shift between *source* and *target* would improve the target performance. The adversarial learning paradigm has been successfully used for person Re-ID, mostly for data augmentation, in both the supervised (standard) [40, 38] and the unsupervised (domain adaptation) [5, 20] learning paradigms.

In this paper, we propose a new method exploiting adversarial strategies for person Re-ID. Our approach is summarized in Figure 1. The intuition behind the core hypothesis in this paper is that camera information, i.e. which camera acquired which image, can be used to learn features that are robust to camera changes and, as a consequence, robust to illumination, background and viewpoint changes. This hypothesis can then be used to transfer information from a labeled person Re-ID source dataset to an unsupervised target dataset. Towards this aim, we propose a method referred to as camera adversarial transfer (CAT). We report experiments on the DukeMTMC-ReID [38] and Market-1501 [35] datasets and discuss the impact of different architectural and methodological choices.

2. Related Work

Most Re-ID models are supervised and employ a single dataset for both learning and testing. A plethora of techniques was proposed in order to improve the performance obtained in this standard setting [34, 14, 11, 4]. These methods fall into two categories. First, metric learning based approaches obtain an optimal representation from the distance between pairs of images [14, 11, 13, 37, 30, 17, 33, 4]. Second, a classifier is trained to return the index of the visible persons [34, 24, 3, 29, 15]. However, independently of the approach employed, these methods perform poorly when the training and the test sets differ significantly in terms of lighting conditions or image quality, as it is the case in cross-dataset experiments [5, 6].

To face this issue, unsupervised cross-dataset person Re-ID methods were recently proposed [6, 32, 23, 5, 28, 12]. By jointly learning on a labeled *source* dataset and an unlabeled *target* dataset, these methods exploit the relatively simple process of gathering unlabeled detections from a *target* camera network. For instance, clustering techniques are used in [6, 32, 20] to infer information about the *target* IDs and to incorporate the estimated IDs into the training procedure. In [23, 12], dictionary learning approaches are proposed in order to learn a dataset-shared representation. Interestingly, some other works [28, 26] employ at-

tribute information available with the source dataset, e.g. gender, haircut or clothing style. They show how exploiting these pieces of information improves the performance in the context of unsupervised person Re-ID, at the cost of manually annotating all these attributes. Recently [21, 22] used spatio-temporal constraints on the target camera network to improve the Re-ID performance.

Some recent work investigated generative adversarial networks (GANs) for learning person Re-ID as a data augmentation/transformation technique. [38] showed that the use of GAN generated images trained on person Re-ID datasets can improve baseline models. In parallel, an image-to-image translation technique is employed in [40] to augment the training dataset by learning the style of each camera in the supervised Re-ID setting. However, such a strategy suffers from a scalability problem when applied to unsupervised person Re-ID, since the number of learned style translations increases exponentially with the number of target cameras. A similar approach is employed in the framework of unsupervised person Re-ID in [5] in order to transfer a *target* style onto labeled *source* detections: by learning the target’s image distribution while preserving the source ID information, they train a generator to match the target data distribution in the image domain and use the transferred images to learn a baseline Re-ID model. Intuitively, our proposed method is similar to this approach: we match domain distributions directly in the feature domain instead of the image domain. In this way, we remove the data generation step, and we unify the learning procedure. More recently, [39] has been proposed to learn each camera style independently and use metric learning approaches to make use of the generated examples and train a Re-ID model.

Adversarial learning for domain adaptation has recently emerged [8, 27, 2]. It aims to train a discriminator to distinguish between *source* and *target* features, such that a feature generator is trained to find a domain-invariant and discriminative representation for the target task. The effectiveness of adversarial domain adaptation for unsupervised person Re-ID has been showed in [8], where a coarse discriminator is trained to distinguish between source and target features, as if they were real and fake samples with a standard GAN.

In order to achieve robustness across camera networks or within a network, we propose to cast the problem in the adversarial framework. Considering a standard person Re-ID model, we take advantage of the adversarial loss to learn an embedding space where the different camera feature distributions match, i.e. they are indistinguishable. To do so, we extend the classic adversarial domain adaptation method to a multiple domain formulation, by using a camera-classifier as discriminator, instead of the usual binary classifier. At the same time, we ensure that our learned features are ID-discriminative by using a classification loss. We demonstrate its interest in the context of unsupervised person re-ID

with a standard baseline. To the best of our knowledge, ours is the first attempt to exploit adversarial learning to directly tackle the data distributions discrepancies related to camera changes in the context of person Re-ID.

3. Camera Adversarial Transfer (CAT)

As previously mentioned, the aim of CAT is to understand whether a camera-wise adversarial strategy could be useful in the context of unsupervised person Re-ID. More formally, let \mathcal{S} denote a source ID-annotated person Re-ID dataset, containing N^S images corresponding to M^S different identities captured by K^S cameras. We write $\mathcal{S} = \{(\mathbf{x}_n^S, \mathbf{p}_n^S, \mathbf{c}_n^S)\}_{n=1}^{N^S}$, where each three-tuple consists of a detection image, \mathbf{x}_n^S , a person ID one-hot vector, $\mathbf{p}_n^S \in \{0, 1\}^{M^S}$ and a camera index one-hot vector, $\mathbf{c}_n^S \in \{0, 1\}^{K^S}$. Similarly, we define $\mathcal{T} = \{(\mathbf{x}_n^T, \mathbf{c}_n^T)\}_{n=1}^{N^T}$ a target person Re-ID dataset, with K^T cameras and N^T element, without ID labels.

Let ϕ be a convolutional neural network front-end (e.g. ResNet-50 to fix ideas) considered as our *feature extractor*. The goal of person Re-ID is to be able to discriminate between identities, and therefore an identity classifier C_{ID} is required. The cross-entropy loss is usually employed:

$$\mathcal{L}_{ID}^S(\phi, C_{ID}) = -\mathbb{E}_{(\mathbf{x}^S, \mathbf{p}^S) \sim \mathcal{S}} \{\log \langle C_{ID}(\phi(\mathbf{x}^S)), \mathbf{p}^S \rangle\}, \quad (1)$$

where \mathbb{E} denotes the expectation and $\langle \cdot, \cdot \rangle$ denotes the scalar product, in this case between the output of the ID discriminator $C_{ID}(\phi(\mathbf{x}^S))$ and the ground-truth ID vector \mathbf{p}^S . Training person Re-ID systems with \mathcal{L}_{ID} loss alone in a supervised setting has been widely studied and can be considered a well-established methodology [5, 38, 40].

In this context, we investigate how to use camera index information to improve the transferability of the learned visual features to a camera-only supervised dataset. One of the main issues is that the features learned with the classical strategy discussed above describe a combination between the identity of the person and camera specifics (such as background, illumination conditions, viewpoint..). Because in the cross-dataset setting the datasets are recorded with different cameras, it results in a significant discrepancy between the two learned feature distributions, and has a strong negative impact on the performance. Formally, this distribution shift can be measured according to the generalized Jensen-Shannon divergence [19],

$$JSD_{1 \leq c \leq K^S + K^T}(p(\phi(X)|C=c)) \neq 0 \quad (2)$$

This is confirmed empirically: we show that when ϕ is trained using (1) only, we can then train a classifier to predict the true camera index from the features of ϕ (see the experimental section).

Recent works in domain adaptation and adversarial learning [10, 8] show that the framework described above can be used for matching the source’s and target’s feature distribution. They do so, first by training a dataset classifier on top of the feature extractor, and then adding an adversarial term in the loss. We inspire from this strategy to propose a multiple domain (camera) discriminator, mixing camera and ID-labels from the source target together with camera-only labels from the target domain.

To implement this, we require a camera index discriminator D_{cam} (see Figure 2 for a complete overview of the architecture) and we define a camera index (cross-entropy) loss:

$$\mathcal{L}_{cam}^{S+T}(\phi, D_{cam}) = -\mathbb{E}_{(\mathbf{x}, \mathbf{c}) \sim \mathcal{S}+\mathcal{T}} \{\log \langle D_{cam}(\phi(\mathbf{x})), \mathbf{c} \rangle\} \quad (3)$$

On one side, the feature extractor must minimize the person Re-ID loss \mathcal{L}_{ID} at the same time as making the problem more challenging for the camera discriminator. On the other side, the camera discriminator tries to learn to identify the camera from which the generated feature $\phi(\mathbf{x}^{S/R})$ has been extracted :

$$\min_{\phi, C_{ID}} \max_{D_{cam}} \mathcal{L}_{ID}^S(\phi, C_{ID}) - \mu \mathcal{L}_{cam}^{S+T}(\phi, D_{cam}), \quad (4)$$

where $\mu > 0$ is a parameter with two possible interpretations. From a domain adaptation perspective, it can be seen as a regularization parameter [8]. From an adversarial learning perspective, μ adjusts the impact of the discriminator’s gradient when training the generator.

Under mild hypothesis, we can show (see Appendix A) that minimizing the loss (4) is equivalent to the following optimization problem

$$\min_{\phi, C_{ID}} \mathcal{L}_{ID}^S(\phi, C_{ID}) \quad (5)$$

s.t. $JSD(p(\phi(x)|c=1), \dots, p(\phi(x)|c=K^S + K^T)) = 0$

Although this adversarial loss could directly be applied to our problem, we empirically show its limitations (cf table 2 in the experimentation section), and propose methods to alleviate its problems in the following sections.

3.1. Domain confusion loss

The adversarial loss as formulated in (4) suffers from convergence problems [10, 1], since the discriminator converges quickly at early stages of the training leading to vanishing gradient problems. The solution usually adopted [10, 27] is to train the generator with a binary crossentropy loss and inverted labels, considering generated images as if their were sampled from the true distribution.

In addition, in the context of our camera adversarial learning, when updating the generator, the adversarial loss

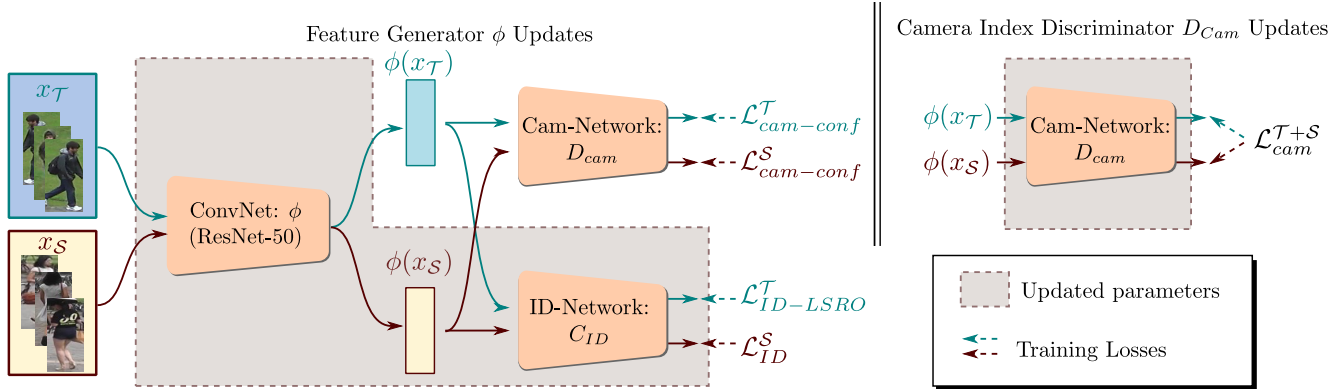


Figure 2. Architecture of our camera adversarial transfer strategy. The generator is first updated using source’s identity labels, and minimize the performance of the camera discriminator, using losses (8) and (9). The discriminator is then updated to recognize from which cameras the feature vectors are extracted with (10).

encourages lower probability values for the true camera labels but does not constrain all the other camera label probabilities to simultaneously increase. Consequently, it is likely that the generator favors the visually closest cameras. Since the visually closest camera usually belongs to the same dataset, this standard adversarial formulation would not force feature distribution matching between the source and target datasets.

To alleviate this problem and inspired by [27], we propose a camera confusion loss by imposing that the feature ϕ results in a uniform distribution labellisation according to the camera-discriminator:

$$\mathcal{L}_{\text{cam-conf}}^{\mathcal{R}}(\phi, D_{\text{cam}}) = -\mathbb{E}_{(\mathbf{x}, \mathbf{c}) \sim \mathcal{R}} \{ \log \langle D_{\text{cam}}(\phi(\mathbf{x})), \mathbf{u} \rangle \}$$

where $\mathcal{R} \in \{\mathcal{S}, \mathcal{T}\}$ and $\mathbf{u} = \frac{1}{K^{\mathcal{S}} + K^{\mathcal{T}}}$ (6)

Note that \mathcal{R} is equal to either \mathcal{S} or \mathcal{T} depending on the current training step as detailed in Sec.3.3. When updating ϕ according to (6), we take into account all the discriminator outputs and therefore encourage the model to match feature distributions across datasets.

It is also close to the alternative adversarial loss described earlier, in the sense that we encourage ϕ to increase all cameras output probabilities instead of only diminishing the true cameras probability output.

3.2. Label smoothing regularization for Outliers

The identity distributions across datasets do not have overlapping support (ie the datasets do not share identity labels). Solving the optimization problem (5) might end up producing features discriminative in terms of source identities, invariant to camera changes, and to target’s identities. It would drastically hurt target’s reidentification performance. To mitigate this problem, we propose to use Label Smoothing Regularization for Outliers (LSRO) [38] for ID

supervision of target’s images.

$$\mathcal{L}_{\text{ID-LSRO}}^{\mathcal{T}}(\phi, C_{\text{ID}}) = -\mathbb{E}_{\mathbf{x}^{\mathcal{T}} \sim \mathcal{T}} \{ \log \langle C_{\text{ID}}(\phi(\mathbf{x}^{\mathcal{T}})), \mathbf{u}_{\text{MS}} \rangle \}$$

$$\mathbf{u}_{\text{MS}} = 1/M^{\mathcal{S}} \quad (7)$$

It has two interpretations: similarly to [38], it acts as a regularization term, introducing appearance variations in the dataset, preventing the ID classifier to focus on under-represented visual features correlated with identities. Second, it prevents the feature distribution matching to crush target’s ID-specific features, by incorporating the information that no target IDs are present in the source dataset, and therefore should lie far for from source’s ID decision boundaries. It aims to mitigate the negative transfer problem.

3.3. Overall training

In practice, both the identity classifier and the camera discriminator are implemented as classification layers within the neural architecture. The difference between them lies on how their weights are updated, i.e. with which information are the classifier and the discriminator trained. From the two optimization problems stated above, we can clearly see that, while the feature extractor is updated with both the identity and the camera losses, the ID classifier and the camera discriminator are updated with the person and camera index information respectively. Even if both, the classifier and the discriminator are classifying/discriminating, only the second is a discriminator within the adversarial philosophy. We end up jointly solving the following optimization

problem

$$\min_{\phi, C_{ID}} \mathcal{L}^S(\phi, C_{ID}, D_{cam}) = \mathcal{L}_{ID}^S(\phi, C_{ID}) + \mu \mathcal{L}_{cam-conf}^S(\phi, D_{cam}), \quad (8)$$

$$\min_{\phi, C_{ID}} \mathcal{L}^T(\phi, C_{ID}, D_{cam}) = \lambda \mathcal{L}_{ID-LSRO}^T(\phi, C_{ID}) + \mu \mathcal{L}_{cam-conf}^T(\phi, D_{cam}), \quad (9)$$

$$\min_{D_{cam}} \mathcal{L}^{S+T}(\phi, C_{ID}, D_{cam}) = \mathcal{L}_{cam}^{T+S}(\phi, D_{cam}), \quad (10)$$

where μ and λ are relevant only when training ϕ .

We optimize those losses iteratively, alternating between the three. We call our method Camera Adversarial Transfer (CAT).

4. Experiments

4.1. Protocol

Datasets. The proposed adversarial transfer strategies are evaluated mainly on two datasets: Market-1501 (Market) [35] and DukeMTMC-reID (Duke) [25, 38]. In both cases, the dataset consists on three parts: a training set, a gallery set and a query set. The query and gallery subparts are never available during training, and only used for testing purposes. The Market dataset is composed of $M = 1,501$ (half for training and half for test) different identities, observed through $K = 6$ different cameras (viewpoints). The deformable parts model [7] is used to detect people in the images. As a consequence we obtain $N = 12,936$ images for training and 19,732 for the gallery images. The query subparts consists of 3,368 hand-drawn bounding boxes. The Duke dataset is composed of $M = 1,404$ (half for training and half for test) identities captured from $K = 8$ different cameras. In addition, 408 other ID, called “distractors”, are added to the gallery. Detections are manually selected, leading to $N = 16,522$ images for train, 17,661 for the gallery and 2,228 queries. Transfer experiments trained on Market and evaluated on Duke are noted Market \rightarrow Duke, and reversely Duke \rightarrow Market.

Evaluation metrics. In order to provide an objective evaluation of the performance of the adversarial strategies, we employ two classical metrics in person Re-ID [35]: Rank-1 (R1) and mean average-precision (mAP). In more details, for each query image, we extract the visual features employing the adversarially learned generator ϕ , and we match them to the features extracted from the images of the gallery using cosine distance. Importantly, the features corresponding to the gallery images captured with the same camera as the query image are not considered. For R1, a query is well identified if the closest gallery feature vector corresponds to the same identity. In the case of mAP, the whole list of gallery images (except those taken with the same camera)

is considered, and the precision of those rank positions in which a positive match is found is averaged. See [35] for details. For both metrics, the mean over the query set is reported.

Implementation and training details. The feature extractor ϕ used in our study corresponds to a recent variant [40] of the well know IDE [36] and denoted by IDE+. IDE is often used as baselines to conduct experimental evaluations for the task of person Re-ID, see [36, 40, 38, 5, 6, 31]. Both architectures are based on ResNet-50, which we implicitly assume pre-trained on ImageNet unless otherwise specified.

In detail, The IDE+ baseline consists in adding the ID classifier after the last pooling layer of ResNet-50 (usually denoted as *pool5*). The ID classifier consists of a hidden fully connected layer of 1,024 units, a batch normalization layer activated with ReLu, a dropout regularization layer (with rate at 0.5), and a fully connected classification layer activated by a softmax function. The number of units of the classification layer depends on the number of training person identities. The overall architecture is trained end-to-end using Stochastic Gradient Descent (SGD).

The camera discriminator consists of one hidden layer of 256 units each, with ReLu activations regularized with weight decay (with rate at 0.01). The camera classification layer is activated with softmax and the number of units depends on the number of cameras of the dataset. An ablation study on the number of units per layer is presented later on in this experimental section. Besides, we faced a practical issue when training the discriminator: it is not a balanced classification problem. In other words, the number of detections per camera strongly depends on the camera (see the supplementary material), and therefore if we do not carefully address this issue, we will be biasing the discriminator towards those cameras in which more people are detected. In order to tackle this problem, we sample evenly across cameras when gathering a batch.

This loss is used to train the networks under the adversarial strategy described earlier. We first resize the input images to 256×128 pixels to keep the aspect ratio. We use mirroring and a batch size of 64 (for the sake of the stability of the results). The pre-training is inspired from [40]. The model is initialized on ImageNet and pre-trained for 20 epochs in the supervised setting (using only source information). The camera matching training is then conducted for 10 epochs, using the same optimization settings. We use a fixed learning rate for all the experiments ($\eta = 0.01$), and use a learning rate multiplier when training the ID branch, which multiplies by 10 the ID classifier’s gradient.

For inference, we use local max pooling (LMP), introduced in [5], which consists in removing the final global average layer of Resnet, and replace it with 2 local max

pooling, one pooling from the half-top of the picture, the other pooling the other part. We therefore obtain a feature vector of dimension 2×2048 .

4.2. Comparison to State of the Art

We compare our results with two hand-crafted feature-based classical strategies: Bag of Words (BoW) [35] and local maximal occurrence (LOMO) [18]. We also compared against clustering and finetuning (PUL) [6] as well as transferable joint attribute-identity deep learning (TJ-AIDL) [28]. Importantly, this method exploits extra labeled data (i.e. attributes) which must be manually annotated and that the rest of the methods do not employ. Results of Bottom-Up Clustering Approach [20] (BUC) are also reported. We compare to the closest work in the literature: SPGAN [5] and HHL [39].

All these results are copied directly from the literature. Table 1 reports the results when using Duke and Market as source and target (left) and vice versa (right).

From Table 1 we can see that deep learning based methods (including ours) outperform hand-crafted features, confirming once more the interest of deep learning for unsupervised person Re-ID. We see that our method yields competitive results compared to the state of the art, getting the best results for the Market \rightarrow Duke (+5% in R1, and + 1.2% in mAP), and second best for Duke \rightarrow Market. We also note that our approach is significantly simpler than SPGAN [5] and HHL [39] (our closest competitive methods) to train, since those methods require first to train a GAN inspired generator to fit target’s image distribution, generate a transferred dataset and then train the baseline on top of it. In a practical point of view, our method is therefore more practical and scalable, since it only requires a few epochs of training from a pretrained network to get competitive results on a new unlabeled dataset.

4.3. Ablation study

Adversarial learning variants We use the adversarial framework to train the model with different training settings. We use the adversarial loss (1) that we denote by adv , to compare with our domain confusion objective (see section 3.1). It best performs for $\mu = 0.01$ and 5 epochs.

We also experiment the classic adversarial domain adaptation setting, when the discriminator is only trained to recognize source’s and target’s features. We call this variant Domain Adversarial Transfer (DAT). Since the task of the discriminator is easier than in the CAT setting, we use a simpler architecture (1 layer, 64 neurons and weight decay at 0.1) to prevent the model to overfit on identities. The best global performances are reported, for $\mu = 0.01$ and 5 epochs.

Finally, we experiment the adversarial setting exploiting only source’s information: the discriminator is only fed

Table 1. R1 and mAP measures on both datasets. The first part of the table is extracted from the literature. All the results are obtained under the same experimental protocol. † refers to unsupervised settings exploiting extra annotations (attributes). Overall best results are shown in **bold**, second best results are in *italic*.

| Method | Duke \rightarrow Market | | Market \rightarrow Duke | |
|------------------|---------------------------|-------------|---------------------------|-------------|
| | R1 | mAP | R1 | mAP |
| BoW [35] | 35.8 | 14.8 | 17.1 | 8.3 |
| LOMO [18] | 27.2 | 8.0 | 12.3 | 4.8 |
| PUL [6] | 45.5 | 20.5 | 30.0 | 16.4 |
| TJ-AIDL [28] † | 57.1 | 26.2 | 39.6 | 22.0 |
| TJ-AIDL [28] † | 58.2 | 26.5 | 44.3 | 23.0 |
| SPGAN [5] | 49.2 | 20.5 | 37.7 | 20.0 |
| SPGAN + LMP [5] | 58.1 | 26.9 | 46.9 | 26.4 |
| BUC [20] | - | - | 47.4 | 27.5 |
| HHL [39] | 62.2 | 31.4 | 46.9 | 27.2 |
| IDE+ | 45.6 | 19.8 | 32.4 | 16.8 |
| IDE+ + LMP | 53.5 | 25.4 | 41.2 | 23.2 |
| CAT + LSRO | 54.9 | 26.2 | 45.9 | 24.6 |
| CAT + LSRO + LMP | 57.8 | 27.8 | 50.9 | 28.7 |

source’s detections, and ϕ is updated using only source’s image, ID and camera labels. We refer to this method as Fully Adversarial Training (FAT). When training this method, we use a 2 layer discriminator of 512 neurons and train it from scratch (pretrained imagenet weights), and train it for 20 epochs. The results of those different variants are reported in table 2. Results with LMP are included for the sake of completeness, but not considered in the following analysis.

All experiments demonstrate asymmetric performances when switching dataset’s role. It generally performs better when considering Duke as target (+13.5% vs +10.3% in best scenarios). An explanation might come from the fact that ID information is closely linked to the camera index information in the Duke dataset, in comparison to the Market. This is backed by the mutual information measure between identities and camera index in each domain: 0.84 for Duke, and 0.14 for Market. It means that providing camera index information will give the model much more identity information in the Duke than in the Market. Therefore, it is more difficult for the model to learn features not dependant on cameras specifics (background/illumination), thus making the features less transferable. It is also confirmed by robustness experiments, developed in the next section.

Second, FAT slightly improves the Re-ID performance compared to our baseline in both cases (+2.7% and 3.8% respectively), without exploiting target information. It confirms the interest for adversarial learning in the context of domain generalization [16].

Interestingly, CAT experiments yield better results than DAT (+7% and +5%). Although DAT experiments use a

Table 2. Adversarial strategies variants. FAT only use source information to train (camera and ID), DAT’s discriminator is supervised only with dataset’s labels, and *adv* refers to the true adversarial loss.

| # exp. setting | Duke→Market | | Market→Duke | |
|------------------|-------------|-------------|-------------|-------------|
| | R1 | mAP | R1 | mAP |
| IDE+ | 45.6 | 19.8 | 32.4 | 16.8 |
| FAT | 48.3 | 20.9 | 36.2 | 19.3 |
| DAT | 45.1 | 19.6 | 37.3 | 19.8 |
| CAT + <i>adv</i> | 49.0 | 21.6 | 42.3 | 22.2 |
| CAT | 52.1 | 24.3 | 43.2 | 23.6 |
| CAT + LSRO | 54.9 | 26.2 | 45.9 | 24.6 |
| CAT + LSRO + LMP | 57.8 | 27.8 | 50.9 | 28.7 |

simpler discriminator, and explicitly enforce a strong regularization, we show that using a labelization less dependant on identities for the discriminator, like camera index, naturally regularizes the discriminator and yield better performance.

Finally, we demonstrate the interest of the camera confusion loss in the context of person Re-ID (+3.1%,+0.9%) and of LSRO (+2.8%,+2.7%).

Robustness and adversarial learning The robustness of the features learned can be easily evaluated, to have a sense of how well camera’s feature distributions match. We split the Gallery (test set) of each dataset into a gallery-training set and a gallery-test set (2/3-1/3). We then train a discriminator (same implementation as in 4.1). We evaluate its camera accuracy performance (the lower the better). Note that the split is done making sure that there is no ID overlap between the 2 gallery sub-datasets, to ensure that we do not use ID-dependent information during the inference.

First of all, we notice that baseline (IDE+) robustness performance is limited, since we manage to train a camera-classifier with good accuracy. It has been the preliminary experiment motivating our adversarial approach. The ID-supervised datasets have better robustness measures, meaning that a classic supervised technique already enforce some kind of robustness, which explain their good performance in a supervised setting.

Second, the Duke dataset consistently has higher accuracy scores across experiments. The camera robustness is tougher to achieve for this dataset, and it comforts our strong ID-camera relationship hypothesis explaining the poorer performance in Duke→Market.

All adversarial experiments encourage camera robustness for both source and target datasets. It is noticeable that FAT achieves it without having access to target information. CAT does a better job than CAT+*adv* in the Duke → Market, which might explain why it outperforms it significantly in Re-ID performance (see table 2). We also note that using LSRO increases the accuracy performance of the cam-

Table 3. Feature’s robustness evaluation: once the model is trained, we extract features from the gallery images of a given dataset, split them into a testing and training set, and train a camera classifier with the latter. We report the accuracy performance on the testing set. Refer the text for detail.

| # exp. setting | Duke→Market | | Market→Duke | |
|------------------|------------------------------|------|-------------|------|
| | Camera classifier’s accuracy | | | |
| IDE+ | 85.5 | 67.6 | 68.2 | 91.0 |
| FAT | 45.5 | 62.0 | 42.7 | 88.0 |
| DAT | 77.6 | 64.4 | 62.8 | 84.4 |
| CAT + <i>adv</i> | 56.4 | 49.1 | 48.1 | 68.1 |
| CAT | 61.0 | 27.9 | 45.4 | 68.6 |
| CAT + LSRO | 71.0 | 33.2 | 50.1 | 68.2 |

Table 4. CAT + LSRO R1 and mAP performance for different number of neurons for the discriminator and μ . We note acc the accuracy performance of the camera discriminator at the end of the training.

| # units | Duke→Market | | | Market→Duke | | |
|---------|-------------|------|------|-------------|------|------|
| | R1 | mAP | acc | R1 | mAP | acc |
| 128 | 52.9 | 24.1 | 35.9 | 44.7 | 23.9 | 30.1 |
| 256 | 54.9 | 26.2 | 31.4 | 45.9 | 24.6 | 33.2 |
| 512 | 50.0 | 22.7 | 43.9 | 43.4 | 23.0 | 32.6 |
| 1,024 | 51.7 | 23.7 | 33.3 | 42.8 | 23.0 | 34.6 |

| μ | Duke→Market | | | Market→Duke | | |
|-------|-------------|------|------|-------------|------|------|
| | R1 | mAP | acc | R1 | mAP | acc |
| 0.01 | 45.0 | 19.4 | 64.3 | 41.4 | 22.2 | 62.3 |
| 0.05 | 48.5 | 21.7 | 44.1 | 45.5 | 24.4 | 40.3 |
| 0.1 | 54.9 | 26.2 | 31.4 | 45.9 | 24.6 | 33.2 |
| 0.2 | 52.9 | 24.8 | 26.5 | 45.3 | 24.7 | 25.6 |

era classifier, indicating that its use mitigates the adversarial strategy impact in order to preserve ID-related information.

Impact of camera variability. We train CAT with different target dataset sizes to understand the impact of the variability of the target dataset on the Re-ID performance. The only modification on the experimental protocol is that the target dataset consists on what is captured from cameras 1 to \tilde{K} , making \tilde{K} vary from 1 (only one camera) to K^T (all cameras). In these experiments we use Market as source dataset, and Duke as target. The gain in performance over the IDE+ baseline is shown in Figure 3.

We first notice that the IDE+ baseline is respectively better, equivalent and worse when using one, two or more than two cameras. Generally, we observe that the Re-ID performance regularly increases with the number of cameras. The regular increase in performance when adding more and more cameras is a clear trend in Figure 3. Our understanding is that the adversarial strategy is good at capturing and exploiting the intra-dataset variability, and satisfactorily ex-

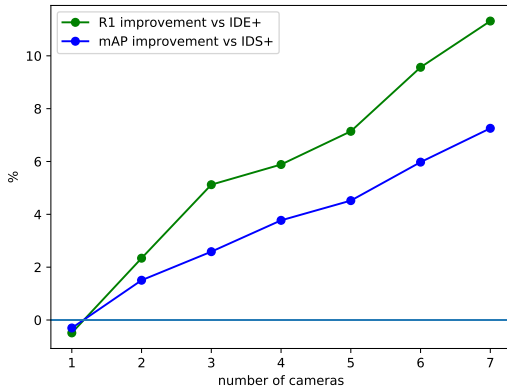


Figure 3. Performance variation with the number of cameras in the setting Market \rightarrow Duke

exploits the different viewpoints to learn more robust and discriminative person Re-ID features. CAT do not only learn to match feature distributions across datasets, but also takes full advantage of the target camera network by matching the different camera distributions.

Impact of the hyper-parameter μ and discriminator architecture. We evaluate the impact of the value of μ on the overall performance of the system in table 4. First of all, we observe that the Re-ID performance is relatively stable when changing the training parameters, although the Duke \rightarrow Market is less stable, more specifically when μ is too low. The Re-ID performance first increases with the adversarial loss weight, and then decrease when it is too strong. Considering the final accuracy of the discriminator, it is conform to intuition. The stronger the adversarial weight gets, the less accurate our discriminator becomes. When comparing the different architectures, we see that an optimal discriminator is found for 258 neurons, and that the Re-ID performance is quite robust to a change of architecture.

Embedding visualization We use the feature embedding to compute a PCA projection of the learned space, and use the first 2 dimensions for visualisation, in Figure 4(a) and 4(b) where both datasets are used for projection, and in Figure 5(a) and 5(b) for target only. We use PCA projection to preserve global structure, which is not guaranteed in other dimensionality reduction methods like t-SNE. The Market \rightarrow Duke setting is used for both, and we use the training sets of each respective dataset. In dataset-wise visualisation, we observe that in the IDE+ setting, using only source information, both distributions visually differs. It fits our strong dataset-shift hypothesis, and motivates our approach. The features learned with CAT have a distribution discrepancy significantly lower, which indicates that

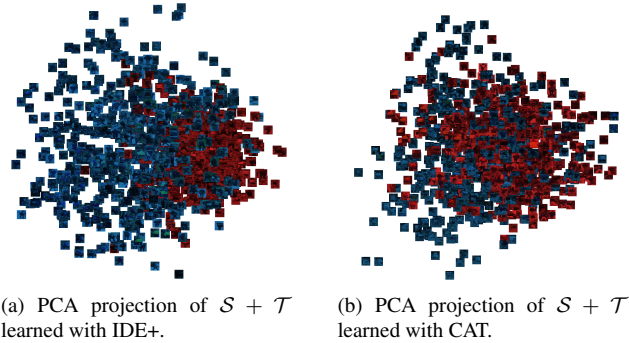


Figure 4. Source dataset is in red and target is in blue. Best viewed in color.

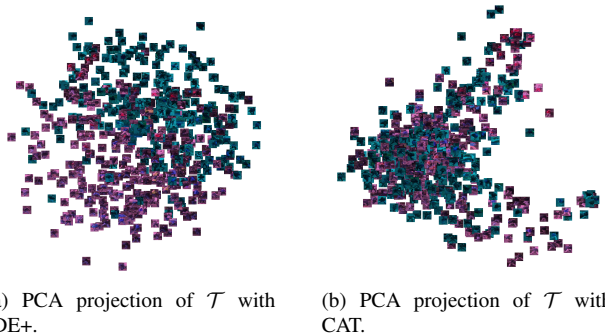


Figure 5. The PCA is only done with target's 7th (purple) and 8th (blue) camera. Best viewed in color.

our approach actively helps to match the 2 domain distributions. Similarly, in the camera-wise visualisation, we observe a stronger separation between cameras when trained with IDE+ than when trained with our adversarial approach. This analysis is backed by the accuracy measures reported in table 3, where we show that we can't train a generalizable camera-classifier, conforing the fact that feature distributions are less separated when learned with CAT. It visually confirms that a camera-based approach improves the results not only because it pushes source and target distribution together, but also matches each camera distribution, especially target's cameras. More visualization are available in the supplementary material.

5. Conclusion

In this paper we addressed the problem of unsupervised person Re-ID. More precisely, we propose to use camera index information within an adversarial paradigm that we name *camera adversarial transfer*. The proposed strategy are compared to several baselines and adversarial variants inspired from the domain adaptation litterature, on the Duke \rightarrow Market and Market \rightarrow Duke experimental settings, thus demonstrating the interest and benefits of exploiting camera index information within an adversarial framework

for person Re-ID. We evaluate different adversarial strategies in terms of person Re-ID performance and camera robustness, discuss the influence of the structure of the camera discriminator as well as the number of cameras and the hyper-parameter μ .

In the future we plan to evaluate the impact of the camera adversarial transfer paradigm in tasks that benefit from robust person Re-ID methodologies, such as multiple person tracking. We would also like to investigate if, together with an auto-encoder, this strategy could be used in a cycled manner, so as to perform robust feature learning and data augmentation for person Re-ID simultaneously.

A. Adversarial learning for multi-domain classifier

In this section, the goal is to prove that optimizing the adversarial loss is equivalent to minimizing the Jensen-Shannon divergence (JSD) between feature distributions across cameras. It relates to the second term of the loss (4) in the main paper. This equivalence has been proved in the original GAN formulation for binary discriminators [10]. We extend the derivation for an arbitrary number of distributions, and to the JSD generalized to multiple distributions.

Let ϕ be our feature extractor, and D_{cam} our camera classifier. Let's define \mathcal{D} as our person Re-ID dataset. It is composed of 3-tuples $(x_n, c_n, p_n)_{n=1}^N$, which correspond to the images, the camera indexes, and the identities, respectively. We also denote with C the number of cameras. Our problem of camera feature distribution matching can be written as the adversarial optimization of

$$\min_{\phi} \max_{D_{cam}} E_{x, c \sim \mathcal{D}} \log D_{cam}(\phi(x))_c \quad (11)$$

During optimization, when the feature extractor ϕ is fixed, the camera classifier D_{cam} is optimized according to:

$$\begin{aligned} \max_{D_{cam}} E_{x, c \sim \mathcal{D}} \log D_{cam}(\phi(x))_c = & \quad (12) \\ \int_x \sum_c p(\phi(x), c) \log(D_{cam}(\phi(x))_c) dx & \end{aligned}$$

For a given image input x , we seek an optimal camera classifier D_{cam}^* with posterior probability d^* , namely

$$d^* = \arg \max_d \sum_{c=1}^C p(\phi(x), c) \log(d) \quad (13)$$

with the constraints $d = (d_1, \dots, d_C) \in \mathbb{R}^C$, $\forall c, 1 \leq c \leq C, 0 \leq d_c \leq 1, \sum_{c=1}^C d_c = 1$ that ensure that d describes a probability distribution. For the sake of notation simplicity, we denote $f(d) = \sum_c p(\phi(x), c) \log(d)$. We also define $\lambda = (\lambda_1, \dots, \lambda_C)$ and $\mu = (\mu_1, \dots, \mu_C)$.

The problem of (13) turns out to be the optimization of the generalized Lagrangian [9], which is written as:

$$\begin{aligned} \max_d \min_{\gamma, (\mu, \lambda \geq 0)} \mathcal{J}(d, \lambda, \mu, \gamma) = & \\ f(d) + \sum_c \lambda_c d_c + \sum_c \mu_c (1 - d_c) + \gamma (\sum_c 1 - d_c) & \quad (14) \end{aligned}$$

$$\nabla_{d_c} \mathcal{J}(d_c^*) = 0 \Leftrightarrow \frac{p(\phi(x), c)}{d_c^*} + \lambda_c - \mu_c - \gamma = 0$$

that leads to

$$\begin{aligned} d_c^* &= \frac{p(\phi(x), c)}{\mu_c - \lambda_c + \gamma} \\ &= \frac{p(\phi(x), c)(d_c^*)(1 - d_c^*)}{\mu_c(d_c^*)(1 - d_c^*) - \lambda_c(d_c^*)(1 - d_c^*) + \gamma(d_c^*)(d_c^* - 1)} \end{aligned}$$

Using the Karush-Kuhn-Tucker property [9], we have $\mu_c(1 - d_c^*) = 0$ and $\lambda_c d_c^* = 0$, thus

$$d_c^* = \frac{p(\phi(x), c)}{\gamma} \quad (15)$$

Due to the constraints of (13), when summing over the camera index c , we obtain:

$$\sum_c d_c^* = \sum_c \frac{p(\phi(x), c)}{\gamma} = 1 \quad (16)$$

where $\gamma = \sum_c p(\phi(x), c)$ is a normalization factor. Therefore the optimal posterior probability is equal to:

$$d_c^* = \frac{p(\phi(x), c)}{\sum_i p(\phi(x), c = i)} \quad (17)$$

After injecting the optimal discriminator D_{cam}^* from (17) above into (11), we obtain:

$$\begin{aligned} \min_{\phi} E_{x, c \sim \mathcal{D}} \log \frac{p(\phi(x), c)}{\sum_i p(\phi(x), c = i)} & \quad (18) \\ = \int_x \sum_c p(\phi(x)|c)p(c) \log \frac{p(\phi(x)|c)p(c)}{\sum_i p(\phi(x), c = i)} dx & \\ = \sum_c p(c) \underbrace{\int_x p(\phi(x)|c) \log p(\phi(x)|c) dx}_{-\sum_c p(c)H(p(\phi(x)|c))} & \\ + \sum_c p(c) \underbrace{\int_x p(\phi(x)|c) \log p(c) dx}_{-H(p(c))} & \\ - \underbrace{\int_x \sum_c p(\phi(x)|c)p(c) \log \left(\sum_i p(\phi(x)|c = i)p(c = i) \right) dx}_{H(\sum_i p(c=i)p(\phi(x)|c=i))} & \end{aligned}$$

We recognize the definition of the JSD in the equation (18), and therefore conclude the proof, solving (11) is equivalent to solving:

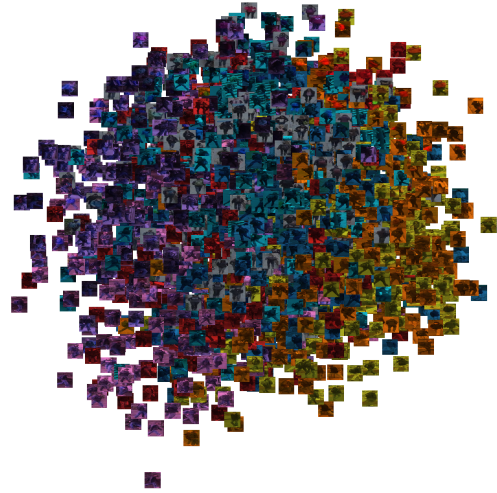
$$\min_{\phi} JSD_{p(c)}(p(\phi(x)|c = 1), \dots, p(\phi(x)|c = C)) \quad (19)$$

where JSD is the generalized Jensen-Shannon divergence between the C distributions $p(\phi(x)|c)$. Note that each distribution $p(\phi(x)|c)$ is weighted by the prior distribution $p(c)$ in the computation of the generalized JSD.

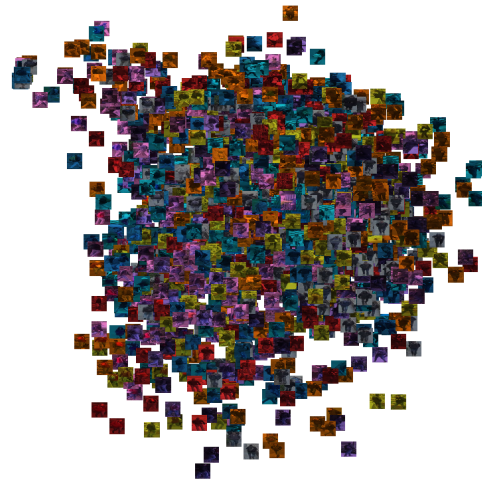
To make sure that each camera distribution $p(\phi(x)|c)$ is considered equally, the prior distribution for each camera should be uniform $p(c) = \frac{1}{N_c}$. It highlights the importance of solving the unbalanced camera-classification problem in our problem. In practice, it is realized by sampling evenly across cameras.

B. Visualization of the Embeddings

We report here further embedding visualization, following the same strategy as described in the main paper. The source dataset is the Market dataset, the target dataset is the Duke dataset. The projection of all cameras is displayed in Figure 6(a) and Figure 6(b), and confirm the hypothesis that target cameras distributions are well separated when using our baseline model (IDE+), contrary the results of our approach (CAT). We also display several camera pairs in Figures 7(a), 7(b), 8(a), 8(b), 9(a) and 9(b). All confirm this hypothesis.

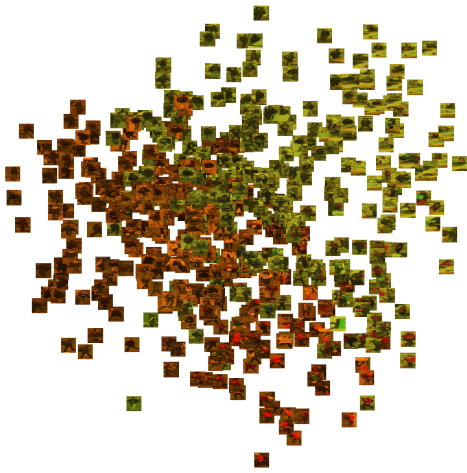


(a) PCA of \mathcal{T} with IDE+ baseline.

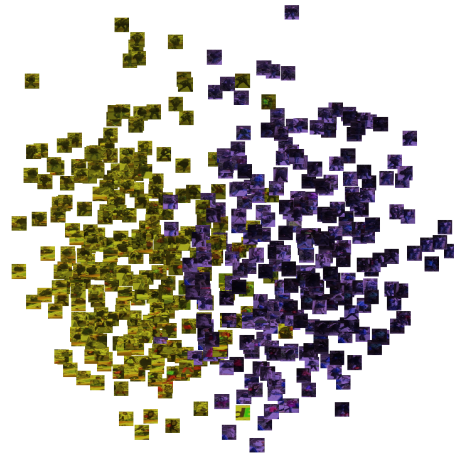


(b) PCA of \mathcal{T} with CAT (Ours).

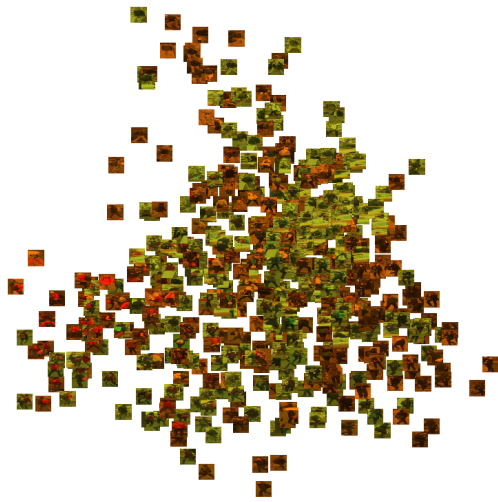
Figure 6. The PCA is only done with all target’s cameras.



(a) PCA of \mathcal{T} with IDE+ baseline.

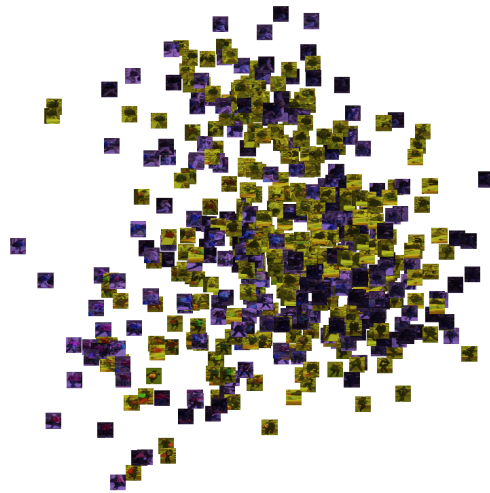


(a) PCA of \mathcal{T} with IDE+ baseline.



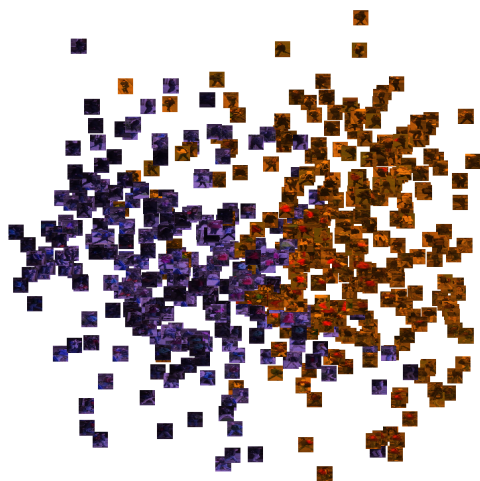
(b) PCA of \mathcal{T} with CAT (Ours).

Figure 7. The PCA is only done with 1st and 2nd target's cameras.

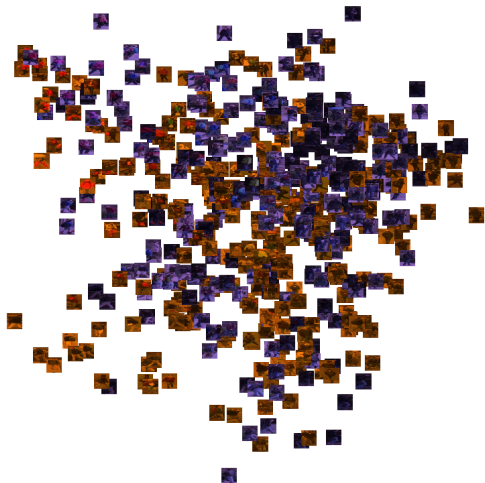


(b) PCA of \mathcal{T} with CAT (Ours).

Figure 8. The PCA is only done with 1st and 3rd target's cameras.



(a) PCA of \mathcal{T} with IDE+ baseline.



(b) PCA of \mathcal{T} with CAT (Ours).

Figure 9. The PCA is only done with 2nd and 3rd target's cameras.

References

- [1] M. Arjovsky and L. Bottou. Towards principled methods for training generative adversarial networks. *CoRR*, abs/1701.04862, 2017. 3
- [2] K. Bousmalis, G. Trigeorgis, N. Silberman, D. Krishnan, and D. Erhan. Domain separation networks. In *NIPS*, 2016. 2
- [3] W. Chen, X. Chen, J. Zhang, and K. Huang. A multi-task deep network for person re-identification. In *AAAI*, 2017. 2
- [4] Y.-C. Chen, X. Zhu, W.-S. Zheng, and J.-H. Lai. Person re-identification by camera correlation aware feature augmentation. *IEEE TPAMI*, 40(2), 2018. 2
- [5] W. Deng, L. Zheng, G. Kang, Y. Yang, Q. Ye, and J. Jiao. Image-image domain adaptation with preserved self-similarity and domain-dissimilarity for person re-identification. In *IEEE CVPR*, 2018. 1, 2, 3, 5, 6
- [6] H. Fan, L. Zheng, and Y. Yang. Unsupervised person re-identification: Clustering and fine-tuning. *CoRR*, abs/1705.10444, 2017. 1, 2, 5, 6
- [7] P. F. Felzenszwalb, R. B. Girshick, D. McAllester, and D. Ramanan. Object detection with discriminatively trained part-based models. *IEEE TPAMI*, 32(9), 2010. 5
- [8] Y. Ganin, E. Ustinova, H. Ajakan, P. Germain, H. Larochelle, F. Laviolette, M. Marchand, and V. Lempitsky. Domain-adversarial training of neural networks. *JMLR*, 17(1), 2016. 2, 3
- [9] I. Goodfellow, Y. Bengio, and A. Courville. *Deep Learning*. MIT Press, 2016. <http://www.deeplearningbook.org>. 9
- [10] I. Goodfellow, J. Pouget-Abadie, M. Mirza, B. Xu, D. Warde-Farley, S. Ozair, A. Courville, and Y. Bengio. Generative adversarial nets. In *NIPS*, 2014. 2, 3, 9
- [11] R. Jin, S. Wang, and Y. Zhou. Regularized distance metric learning: Theory and algorithm. In *NIPS*, 2009. 2
- [12] E. Kodirov, T. Xiang, and S. Gong. Dictionary learning with iterative laplacian regularisation for unsupervised person re-identification. In *BMVC*, 2015. 1, 2
- [13] M. Koestinger, M. Hirzer, P. Wohlhart, P. M. Roth, and H. Bischof. Large scale metric learning from equivalence constraints. In *IEEE CVPR*, 2012. 2
- [14] W. Li, R. Zhao, T. Xiao, and X. Wang. Deepreid: Deep filter pairing neural network for person re-identification. In *IEEE CVPR*, 2014. 1, 2
- [15] W. Li, X. Zhu, and S. Gong. Person re-identification by deep joint learning of multi-loss classification. *IJCAI*, 2017. 2
- [16] Y. Li, X. Tian, M. Gong, Y. Liu, T. Liu, K. Zhang, and D. Tao. Deep domain generalization via conditional invariant adversarial networks. In *The European Conference on Computer Vision (ECCV)*, 2018. 6
- [17] S. Liao, Y. Hu, X. Zhu, and S. Z. Li. Person re-identification by local maximal occurrence representation and metric learning. In *IEEE CVPR*, 2015. 2
- [18] S. Liao, Y. Hu, X. Zhu, and S. Z. Li. Person re-identification by local maximal occurrence representation and metric learning. In *IEEE CVPR*, 2015. 6
- [19] J. Lin. Divergence measures based on the shannon entropy. *IEEE Transactions on Information Theory*, 1991. 3
- [20] Y. Lin, X. Dong, L. Zheng, Y. Yan, and Y. Yang. A bottom-up clustering approach to unsupervised person re-identification. In *AAAI Conference on Artificial Intelligence (AAAI)*, 2019. 2, 6
- [21] J. Lv, W. Chen, Q. Li, and C. Yang. Unsupervised cross-dataset person re-identification by transfer learning of spatial-temporal patterns. In *IEEE CVPR*, 2018. 2
- [22] L. Minxian, Z. Xiatian, and G. Shaogang. Unsupervised person re-identification by deep learning tracklet association. In *ECCV 2018*, 2018. 2
- [23] P. Peng, T. Xiang, Y. Wang, M. Pontil, S. Gong, T. Huang, and Y. Tian. Unsupervised cross-dataset transfer learning for person re-identification. In *IEEE CVPR*, 2016. 1, 2
- [24] X. Qian, Y. Fu, Y.-G. Jiang, T. Xiang, and X. Xue. Multi-scale deep learning architectures for person re-identification. In *IEEE ICCV*, 2017. 2
- [25] E. Ristani, F. Solera, R. Zou, R. Cucchiara, and C. Tomasi. Performance measures and a data set for multi-target, multi-camera tracking. In *ECCV Workshops*, 2016. 5
- [26] C. Su, S. Zhang, J. Xing, W. Gao, and Q. Tian. Deep attributes driven multi-camera person re-identification. In *ECCV*, 2016. 2
- [27] E. Tzeng, J. Hoffman, K. Saenko, and T. Darrell. Adversarial discriminative domain adaptation. In *IEEE CVPR*, 2017. 2, 3, 4
- [28] J. Wang, X. Zhu, S. Gong, and W. Li. Transferable joint attribute-identity deep learning for unsupervised person re-identification. In *IEEE CVPR*, 2018. 1, 2, 6
- [29] T. Xiao, H. Li, W. Ouyang, and X. Wang. Learning deep feature representations with domain guided dropout for person re-identification. In *IEEE CVPR*, 2016. 2
- [30] F. Xiong, M. Gou, O. Camps, and M. Sznai. Person re-identification using kernel-based metric learning methods. In *ECCV*. Springer, 2014. 2
- [31] M. Ye, A. J. Ma, L. Zheng, J. Li, and P. C. Yuen. Dynamic label graph matching for unsupervised video re-identification. In *IEEE ICCV*, 2017. 5
- [32] H.-X. Yu, A. Wu, and W.-S. Zheng. Cross-view asymmetric metric learning for unsupervised person re-identification. In *IEEE ICCV*, 2017. 1, 2
- [33] L. Zhang, T. Xiang, and S. Gong. Learning a discriminative null space for person re-identification. In *IEEE CVPR*, 2016. 2
- [34] H. Zhao, M. Tian, S. Sun, J. Shao, J. Yan, S. Yi, X. Wang, and X. Tang. Spindle net: Person re-identification with human body region guided feature decomposition and fusion. In *IEEE CVPR*, 2017. 1, 2
- [35] L. Zheng, L. Shen, L. Tian, S. Wang, J. Wang, and Q. Tian. Scalable person re-identification: A benchmark. In *IEEE ICCV*, 2015. 1, 2, 5, 6
- [36] L. Zheng, Y. Yang, and A. G. Hauptmann. Person re-identification: Past, present and future. *CoRR*, abs/1610.02984, 2016. 1, 5
- [37] W.-S. Zheng, S. Gong, and T. Xiang. Reidentification by relative distance comparison. *IEEE TPAMI*, 35(3), 2013. 2
- [38] Z. Zheng, L. Zheng, and Y. Yang. Unlabeled samples generated by gan improve the person re-identification baseline in vitro. In *IEEE ICCV*, 2017. 1, 2, 3, 4, 5

- [39] Z. Zhong, L. Zheng, S. Li, and Y. Yang. Generalizing a person retrieval model hetero- and homogeneously. In *The European Conference on Computer Vision (ECCV)*, September 2018. [2](#), [6](#)
- [40] Z. Zhong, L. Zheng, Z. Zheng, S. Li, and Y. Yang. Camera style adaptation for person re-identification. In *IEEE CVPR*, 2018. [1](#), [2](#), [3](#), [5](#)